


RESEARCH

Open Access



Optimizing biochar-based geopolymer composites for enhanced water resistance in asphalt mixes: an experimental, microstructural, and multi-objective analysis

Nura Shehu Aliyu Yaro^{1,2*} , Muslich Hartadi Sutanto¹, Noor Zainab Habib³, Aliyu Usman^{1,2}, Liza Evianti Tanjung¹, Ibrahim Aliyu² and Ahmad Hussaini Jagaba⁴

*Correspondence:
nura_19001733@utp.edu.my

¹ Department of Civil and Environmental Engineering, Universiti Teknologi PETRONAS, Bandar Seri Iskandar, Perak 32610, Malaysia

² Department of Civil Engineering, Ahmadu Bello University, Zaria, Kaduna State 810107, Nigeria

³ Heriot-Watt University, Dubai International Academic City, P. O. Box, Dubai 294345, United Arab Emirates

⁴ Interdisciplinary Research Centre for Membranes and Water Security, King Fahd University of Petroleum and Minerals, Dhahran 31261, Saudi Arabia

Abstract

Due to increased traffic and environmental concerns, this study addresses challenges in conventional asphalt concrete. Our focus is on enhancing the water resistance of asphalt mixes through the optimization of both the asphalt binder and the biochar-based geopolymer composite. We employ experiments and response surface methodology to assess their impact on volume, Marshall parameters, and water resistance. Asphalt binders were evaluated within the range of 4–6%, while biochar-based geopolymer composite levels varied from 0 to 4%. According to the findings, the incorporation of the biochar-based geopolymer composite improves asphalt properties, stiffness, and temperature sensitivity. Response surface methodology (RSM) was utilized to construct robust mathematical models with high R^2 values (90%) and low p -values. Multi-objective optimization indicated that optimal content levels were 4.56% for the binder and 2.71% for the biochar-based geopolymer composite. Model accuracy was confirmed with less than a 5% error in validation tests. The research also identified structural changes in the asphalt binder caused by the BGC Si–O phase. Additionally, the leaching value for both BGC and BGC-MAB asphalt concrete was found to be substantially below the regulatory limit, demonstrating the environmental safety of incorporating BGC into the asphalt sector.

Keywords: Water damage, Biochar-based geopolymer composite, Response surface methodology, Asphalt concrete, Leaching, Environmental sustainability

Introduction

Asphalt concrete, also known as asphalt pavement, is commonly used in highway construction due to its high load-bearing capacity and durability [1]. However, deformation, fissures, and water damage jeopardize its structural integrity, necessitating ongoing maintenance. Furthermore, water damage is regarded as a major factor that contributes to premature failure in asphalt concrete, emphasizing the need for special consideration during the design stage [2]. Due to increased highway traffic, researchers are exploring

new ways to enhance longevity and sustainability [3, 4]. The performance of asphalt mixes is significantly influenced by the asphalt binder. Therefore, proper bonding capability within the asphalt pavement is crucial for optimal performance over its service life. External and environmental factors contribute to asphalt binder aging, impacting its performance [5]. Consequently, various asphalt modifiers, such as minerals or polymers, have been demonstrated to improve pavement properties [5, 6]. Polymer additives, while effective, are often costly and require high-temperature processing [7]. In contrast, natural material additives offer several advantages, including improved bonding between the binder and crushed stones, increased pavement durability, simpler production methods, lower costs, good performance, and abundant sources [3, 7]. Consequently, pavement researchers increasingly advocate for the use of alternative material modifiers to enhance the properties of both the asphalt binder and mixture [8]. Due to growing concerns about environmental sustainability and the imperative for a more sustainable pavement industry, researchers and engineers continually seek new materials and methods to enhance the durability and lifespan of asphalt concrete roadways [9, 10]. One promising approach that has garnered significant attention is the utilization of biochar-based geopolymer in asphalt concrete. This innovative method combines the advantages of biochar, a carbon-rich biomass pyrolysis residue, and geopolymer, a sustainable and adaptable alternative to conventional modifiers. Water in asphalt poses a nuanced challenge to its structural integrity, potentially leading to a loss of stiffness in the asphalt pavement and, consequently, jeopardizing the overall road structure [11]. While moisture is not directly responsible for all road distress, its presence exacerbates the extent and severity of pre-existing problems, such as permanent deformation, fatigue, and pavement degradation [11].

Biochar, which is produced by the thermal decomposition of organic waste materials, has several advantageous properties for asphalt pavement applications. Its high carbon concentration provides exceptional stability and strength, while also improving rutting and cracking resistance [9]. Biochar serves as a carbon sink and aids in the reduction of greenhouse gas emissions [9, 12]. Biochar's adsorption capabilities resist moisture issues, resulting in long-lasting, sustainable pavement. Zhou and Adhikari [13] added biochar at varying dosages of 2%, 4%, 6%, and 8% into the bio-oil binder and the study outcomes show that biochar improved blend flow-induced crystallization and performance. Also, Çeloğlu et al. [14] employed walnut and apricot shell biochar by 5%, 10%, and 15% as bitumen modifiers at 180 °C; they observed that biochar enhances the binder stiffness at high temperatures. Another research by Ghasemi et al. [15] studied the use of biochar and hydrochar as anti-aging agents in bitumen blends and it was observed that the algal biochar increased anti-aging properties, while the hardwood biochar decreased viscoelasticity-based aging. Thus, based on prior studies, it has been observed that the use of biochar in asphalt binder has advantages such as increased durability, aging resistance, reduced pavement distress, and reuse of waste [9]. Also, based on work of literature, biochar has poor storage stability and there are still limited studies on the long-term water damage of the biochar-modified mixture. On the other hand, geopolymer is a cementitious substance created by activating aluminosilicate precursors with alkaline activators, such as fly ash or slag [16]. In comparison to traditional cement-based binders, geopolymer offers exceptional mechanical strength, chemical resistance, and durability [17].

Geopolymer fillers improve asphalt mixes. In an investigation performed by Ismail [18], fly ash geopolymer filler enhanced porous asphalt stability and stiffness, outperforming traditional flexible pavement. The outcome also revealed that geopolymer-modified flexible pavement had higher creep stiffness and permanent deformation resistance than unmodified flexible pavement. Also, Ahyudanari et al. [19] found that flexible pavement modified with geopolymer as a filler was more stable than unmodified flexible pavement. Also, Aditama et al. [20] investigated aggregate grade improvements in geopolymer-modified flexible pavement utilizing fly ash-based geopolymer. Furthermore, Yaro et al. [21] investigated oil palm waste powder as a geopolymer addition, resulting in stiffer, less penetrable, and better-softened asphalt with greater stability. In addition, a study by Jameel et al. [22] looks into the use of two different bio-oils in recycled asphalt pavement mixtures to revitalize aged bitumen. According to the findings of the study, these oils improve the resistance of mixtures to low-temperature cracking, water damage, and rutting. From the work literature, it was observed that using geopolymers in asphalt mixtures improves mechanical properties, increases durability, and promotes sustainability by increasing stiffness, strength, and resistance to aging [23]. Although geopolymers have many advantages, more research is necessary on the long-term water damage of the biochar-modified mixture to fully realize these benefits due to application challenges and the need for optimized mix design.

The use of geopolymer and biochar in flexible pavement is gaining popularity as a means to enhance pavement quality while reducing environmental impact [24]. While prior research has predominantly concentrated on individual elements, this study utilizes response surface methodology (RSM) and central composite design (CCD) to explore their interactions. ANOVA will be employed to evaluate these interactions and individual effects, with volumetric and Marshall tests influencing the analysis of asphalt concrete design. This comprehensive method seeks to enhance our comprehension of parameter interactions, particularly in the realm of water damage resistance, which has received less attention in the past. This approach aims to result in better-performing asphalt concrete. The study complies with numerous Sustainable Development Goals (SDGs) as it will contribute to Goal 9 by concentrating on developing sustainable and resilient infrastructure via asphalt mixture modification. Goal 11 is also addressed by attempting to create safe and sustainable transit networks, which are critical for metropolitan residents. The study also contributes to Goal 12 by promoting responsible consumption and production practices in the asphalt operations, notably in managing chemicals and wastes. Furthermore, Goal 13 is targeted because the research incorporates climate change mitigation techniques in asphalt materials. Finally, the study's interdisciplinary and multi-objective approach aligns with Goal 17 by encouraging partnerships for sustainable development, emphasizing the importance of global collaboration in advancing sustainable paving solutions.

The purpose of this study is to ascertain the combined impact of biochar and geopolymer on the performance of asphalt concrete. It addresses a gap by evaluating the water damage resistance of the biochar-based geopolymer composite (BGC) as an asphalt modifier. The objective is to assess whether BGC can enhance water-induced damage resistance in asphalt concrete, employing both experimental and statistical methodologies.

Methods

Asphalt binder and aggregates

The asphalt binder utilized in this study was procured from the PETRONAS petrochemical plant and possessed a penetration grade of 80/100. Table 1 presents the physical properties of the asphalt binder. Crushed granite sourced from a nearby quarry was employed in the study. The aggregate selection and testing adhered to the Malaysian Public Works Department (PWD) standards for asphalt concrete construction [25]. Table 1 details the physical properties of the aggregate, demonstrating compliance with the specified parameters. Granitic dust, passing through a standard 75 μm filter size, served as the mineral filler.

Biochar-based geopolymer material preparation

A local Malaysian chemical laboratory supplied high-quality chemicals and reagents for the study, including sodium and potassium phosphate buffer powder, sodium hydroxide (NaOH), potassium hydroxide (KOH), and hydrochloric acid (HCl). Indigenous businesses provided palm oil fuel ash (POFA) and waste rice straws. POFA, metakaolin, and sodium metasilicate were all utilized, each containing amorphous aluminosilicate. The POFA underwent thorough cleaning, removal of moisture, crushing, and sieving (75 μm) on a RETSCH AS-200 sieve shaker, with a calculated specific gravity of 1.298 kg/m^3 . Metakaolin, the fundamental raw material of geopolymers, originated from locally available kaolin and was calcined at 750 $^{\circ}\text{C}$ for 5 h in this study. After cooling for 24 h, the

Table 1 Conventional characteristics of asphalt binder, aggregate, and BGCG

Properties	Standard	Units	Values	Range
<i>Asphalt binder</i>				
Softening point	ASTMD36-12	$^{\circ}\text{C}$	49.5	45–52
Ductility at 25 $^{\circ}\text{C}$	ASTM D113-07	cm	114	>100
Penetration	ASTMD5-13	dmm	87	80–100
Mass loss	ASTM D2872	%	0.03	-
Specific gravity	ASTMD70-18	-	1.022	1.0–1.05
<i>Fine aggregate</i>				
Flat and elongated tests	ASTM D 4791	%	18.2	
Bulk specific gravity	ASTM C 128	g/cm^3	2.54	
Absorption	ASTM C 127	%	1.19	<2
<i>Coarse aggregate</i>				
Flakiness	BS 812 Part 105.1	%	9.2	<20
Absorption	ASTM C 127	%	0.58	<2
Bulk specific gravity	ASTM C 127	g/cm^3	2.83	
Aggregate crushing value	BS 812- 110	%	20.05	<30
Abrasion loss	ASTM C 131	%	22.68	
Elongation	BS 812 Part 105.2	%	12.48	<20
<i>Biochar-based geopolymer composites</i>				
Color	Dusky gray			
Moisture content	ASTM D2216-71	%	1.04	
Specific surface area	ASTM C1274—12	m^2/g	1.1027	-
Specific gravity	ASTM C188-17	g/m^3	2.62	-
Loss on ignition (LOI)	ASTM C311-17	%	9.87	-

calcined kaolin was incorporated into the geopolymerization process alongside POFA as a filler. To minimize contaminants from rice straw preparation, washing with tap water was conducted. The straw underwent soaking in a mineral water solution (1 L/100 g) overnight, followed by rinsing, air-drying at 110 °C for a day, and pulverization to 75 µm fine particles using a mechanical ball mill machine. This prepared material served as the starting point for biochar synthesis.

Waste-derived biochar-based geopolymer composites preparation

The waste-derived POFA metakaolin geopolymer was created by combining 20 g of both components in a 1:1 ratio. An alkali-activator, serving as a binder and solvent for removing surface contaminants, was generated by immersing solid sodium metasilicate (Na_2SiO_3) in deionized water (10 g). The correct amount of sodium metasilicate was determined using an attrition measuring process. To produce homogeneous geopolymer gels, approximately 60% of the weight in water was added, and the activator was mixed into the powdered mixture. These gels were then molded into 50 × 50 × 50 mm cubic molds and solidified in a valve bag for 24 h. Subsequently, the geopolymer blocks were cured in an oven at 80 °C for 2 days before undergoing immersion in water for an additional 3 days to further cure. The obtained powder was crushed and sieved to a size passing 75 µm, and the filtrate was collected and continuously washed with deionized water to achieve a pH of 7.5–8.0 [26]. By combining rice straw with POFA/metakaolin geopolymer, a biochar-based geopolymer composite was produced (Fig. 1). The method involved combining 10 g of rice straw-based biochar (RSB) with 15 g of POFA metakaolin geopolymer (PMG), then adding 8 g of KOH as an alkali-activator. To ensure optimal homogeneity, the RSB and PMG combination was pulverized using a porcelain ball grinder after the geopolymer synthesis technique. The resulting mixture was sieved through 75 µm, and the filtrate was used in this study as an asphalt binder additive.

Characterization

This investigation encompassed chemical and microstructural analyses. To determine the chemical composition of BGC, the Bruker XRF model S8 Tiger X-ray fluorescence (XRF) analyzer was employed. Additionally, the crystallinity and mineralogy phases of both BGC and BGC-MAB were examined using qualitative X-ray diffraction (XRD) with a Bruker AXS D8 advance, and the XRD peaks were analyzed using the High Score Plus analytical program. FTIR spectroscopy was utilized to assess the chemical properties of the asphalt binder and BGC. The Perkin Elmer Spectrum 65 FT-IR spectrometer from MA, USA, was employed for this purpose. This spectroscopic approach characterized the structural properties of both the control and BGC-modified asphalt binder (BGC-MAB) and evaluated the chemical properties of BGC. Surface morphology of the BGC and modified asphalt binder was examined using SEM/EDX. The SEM–EDX investigation utilized a detailed scanning electron microscope (Carl Zeiss model SUPRA 55VP, EVO LS15, Germany).

BGC-modified asphalt binder preparation and conventional test

The BGC-modified asphalt binder (BGC-MAB) was produced through a series of carefully controlled steps using a high-shear laboratory blender. Initially, the

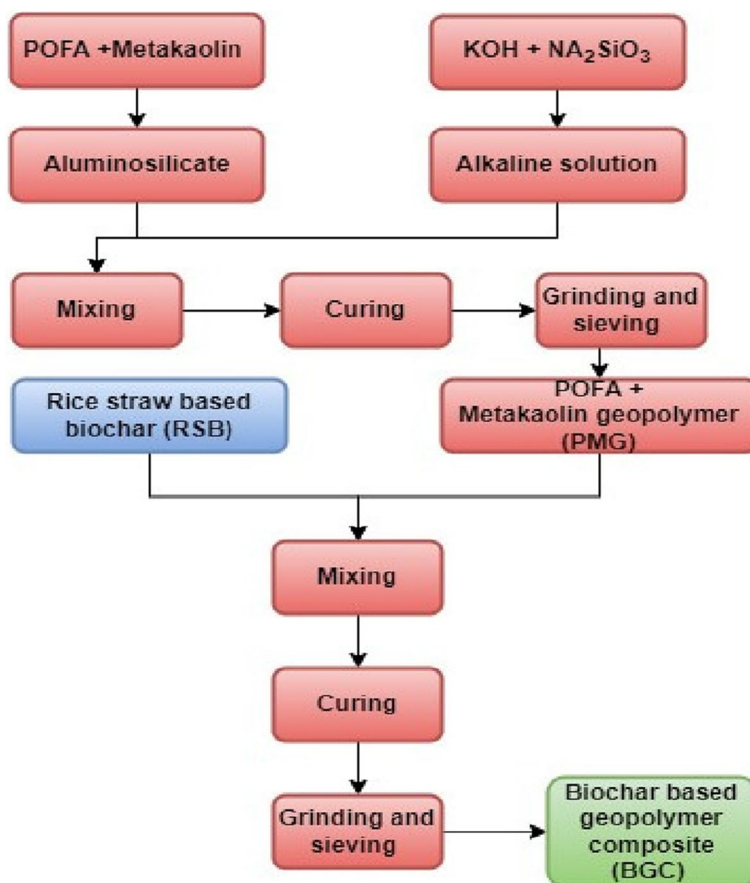


Fig. 1 Biochar-based geopolymer composite preparation

penetration grade 80/100 asphalt binder underwent preheating in an oven at 110 °C to achieve the desired viscosity for subsequent modification and mixing. The precisely measured control asphalt binder was then placed in an aluminum container. Incorporation of BGC into the asphalt binder was a meticulous process to prevent clustering during mixing, ensuring the proper proportion relative to the weight of the control asphalt binder. A mechanical blender with a blending speed of 1250 rpm facilitated the mixing process, lasting 60 min at 155 °C. The objective was to create a homogeneous BGC-MAB blend with POCF particles uniformly dispersed throughout the asphalt binder matrix. To assess the asphalt binder blend, standard test methods were employed as evaluation criteria, providing insights into the blend’s characteristics and performance. The comparison of the performance between the control asphalt binder and BGC-MAB blends adhered to relevant standards. Penetration values, in accordance with ASTM D5, and softening points, determined per ASTM D36, were measured. Temperature sensitivity was examined using the penetration index (PI) to evaluate bitumen performance across various temperatures. Additionally, ductility tests were conducted following ASTM D113. A storage stability test was carried out to evaluate the high-temperature stability of the control asphalt binder and BGC-MAB

blends during storage. The tube test method specified in PN-EN 13399 was employed, allowing an assessment of the asphalt binder’s long-term storage stability.

Asphalt concrete preparation

The Marshall mix design was employed to ascertain the optimal asphalt binder content and enhance the control asphalt concrete, adhering to the ASTM D692 standard [27]. Dense-graded asphalt concrete with a nominal maximum aggregate size of 14 mm (AC14) was used in the study, and Fig. 2 illustrates the aggregate gradation based on PWD standards. To determine the optimal asphalt binder content (OAC), three samples were prepared with varying proportions of asphalt binder (4.0%, 4.5%, 5.0%, 5.5%, and 6.0% by weight of the asphalt concrete). A Marshall compactor was utilized for compaction, applying 75 hits per face to achieve the desired compaction. Following compaction, the samples, approximately 101 mm in diameter and 63.5 mm in thickness, were carefully placed on a smooth surface. They were left undisturbed at room temperature overnight for optimal conditioning before subsequent testing. This overnight conditioning ensured consistent and accurate results during testing the following day. Before initiating performance testing, the asphalt concretes were analyzed at the OBC for volumetric and Marshall parameters. The Malaysian PWD has established an AC14 range for all asphalt concrete [25], confirming adherence to the volumetric property criteria mandated by the regulatory body. This step validated that the asphalt concrete met the required standards set by the regulatory authority.

Volumetric and Marshall parameters

This study investigates the engineering parameters of asphalt mixes, including bulk specific density (BSD), air voids (AV), voids filled with asphalt binder (VFA), voids filled with mineral aggregates (VMA), Marshall stability, and flow. The selection of these properties was deliberate, as they offer crucial insights into the volumetric and structural aspects of asphalt concrete. The objective of the study was to assess the performance of asphalt concrete modified with BGC-MAB, specifically focusing on structural integrity and compaction characteristics through the analysis of these properties.

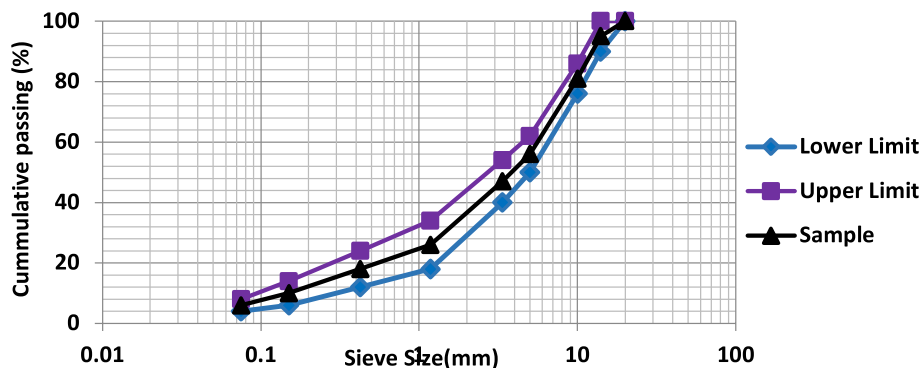


Fig. 2 Asphalt concrete AC14 aggregate gradation based on PWD

Moisture damage test

In the study, the modified Lottman test (AASHTO T283) was employed to evaluate the water damage sensitivity of asphalt concrete based on indirect tensile strength (ITS). Marshall samples were created for both dry and wet conditions. ITS was calculated using peak load data, and the ITS ratio (ITSR) served as the metric to gauge susceptibility to water damage. This ratio indicated the extent of water-induced damage in the asphalt concrete. Equation 1 was utilized to calculate the ITS of the asphalt concrete, where ITS represents indirect tensile strength (kPa), F_{Max} signifies the maximum applied vertical load (kN), h denotes sample thickness, and d denotes average sample diameter (mm). To determine the asphalt concrete’s water susceptibility, the ITS ratio (ITSR) of the conditioned samples was compared to the dry samples for each type of asphalt concrete. Equation 2 was applied to calculate the ITSR, providing a quantitative measure to assess water damage in asphalt concrete.

$$ITS = \frac{2 \times F_{Max}}{\pi \times h \times d} \tag{1}$$

$$ITSR = \frac{ITS_{Wet}}{ITS_{Dry}} \times 100 \tag{2}$$

RSM-based experimental design

RSM serves as a proficient mathematical tool for designing, analyzing, optimizing, and verifying experiments. In this study, Design-Expert® software version 13.1.0 was employed to create experimental designs, establish links between input variables and responses, and generate visual representations of the data. The CCD method was selected for its effectiveness in illustrating the relationship between input components and their corresponding responses [28–31]. The study investigates the impact of BCG and asphalt binder content on various engineering parameters of asphalt concrete, including BSD, AV, VFA, VMA, Marshall stability, flow, and ITSR (water damage). The coded and actual values of the input variables are presented in Table 2.

Following the CCD methodology, the pertinent input factors for predicting the anticipated outcomes were identified and incorporated into a suitable polynomial model. Equation 3 presents a generalized equation that predicts the responses through a second-order polynomial equation, which was utilized to assess the model.

$$Y = \beta_0 + \sum_{p=1}^z \beta_p X_p + \sum_{p=1}^z \sum_{q \geq p}^z \beta_{pq} X_p X_q + \varepsilon \tag{3}$$

Table 2 Input variable coded and actual range

Input factors	Coded level		
	−1	0	+1
A: asphalt binder content (%)	4	5	6
B: BGC content (%)	0	2	4

where Y is the predicted variable, β_0 is the design center point fixed response value, X_p and X_q are input factors, β_p is the linear coefficient, β_{pq} is the interactive coefficient, where r and m are the linear and quadratic coefficients, z is the number of variables, and ε represents the model error.

As depicted in Table 3, a total of 13 experimental runs were established using RSM for the experimental design. For enhanced reliability, the central point was replicated five times, encompassing low and high levels of significant factors under evaluation. Randomization and potential bias were tested three times. After entering the data into the RSM program, it was cross-checked with response variables before being modeled and optimized. ANOVA was employed to assess the model's predictive capability, utilizing p -values and F -values at a 95% confidence level to evaluate the lack of fit (LoF) and overall appropriateness of the model [32]. The F -test was utilized to gauge the model's adequate precision (AP), standard deviation (SD), and reproducibility, employing the coefficient of variation (C.V). RSM models were visually represented using 3D plots to emphasize interactions between input factors. Within the RSM framework, numerical optimization unveiled optimum parameters, subsequently validated through additional experiments to showcase the accuracy and reliability of the RSM results.

The effect of water immersion on the durability performance of asphalt concrete

The ITSr tests were conducted under varying immersion periods to assess the durability properties of both the control and BGC-MAB asphalt concrete. These experiments aimed to gauge the performance of asphalt concrete at different stages, specifically during the dry phase and immersion phase. For the durability testing, two sets of samples, representing the control and BGC-MAB asphalt concrete, were prepared, and exposed to different conditioning periods. The first set comprised dry samples maintained at room temperature. In the second batch, water-conditioned asphalt concrete specimens were submerged for 1, 2, 4, and 6 days. Adhering to the AASHTO T28 standard, the asphalt concretes were immersed in water for 5–10 min under a vacuum to attain a saturation limit of 70–80%. The conditioning periods for all asphalt concrete specimens followed AASHTO T28 recommendations, ensuring uniform testing conditions throughout the experiment. Notably, all specimens subjected to different conditioning times achieved a saturation limit within the normal range of 70–80%, ranging from 73 to 77%. Following 1 day of conditioning, the specimens were immersed in a water basin set at 60 ± 1 °C for an additional day. Subsequently, they were evaluated after an additional 2 h of conditioning in another immersion bath maintained at 25 ± 1 °C. Wet samples, subjected to extended conditioning times, were immersed in a 25 ± 1 °C water bath for 24 h less than the stipulated time. They were then placed in a water basin set to 60 ± 1 °C for 1 day before undergoing testing. At the conclusion of each water immersion period, the specimens were removed from the water for testing.

Leaching analysis

The assessment of the environmental impact stemming from the inclusion of BGC-MAB in asphalt concrete holds paramount importance for the safety of asphalt pavement. The USEPA 1311 standard methodology, along with the toxicity characteristic leaching procedure (TCLP), was employed to scrutinize the mobility of heavy metals and other

Table 3 RSM-CCD experiment design matrix and responses

Run	Input factors		Responses							
	Asphalt binder (%)	BCG (%)	BUW	VTM (%)	VFB (%)	VMA (%)	Stability (kN)	Flow (mm)	ITS (kPa)	ITSR (%)
1	5	2	2.443	4.28	74.36	16.02	14.47	3.03	1433	93.53
2	5	2	2.445	4.37	74.21	16.06	14.53	2.94	1429	90.69
3	4	4	2.448	4.02	90.88	16.54	15.19	2.81	1246	78.33
4	4	2	2.436	4.95	66.75	17.16	13.75	2.82	1376	87.13
5	5	2	2.438	4.52	76.27	15.98	14.37	2.97	1413	89.53
6	4	0	2.411	5.11	60.71	17.38	13.98	2.85	1114	64.43
7	6	2	2.429	4.13	81.55	17.24	13.71	3.21	1143	71.48
8	5	2	2.441	4.41	79.21	16.15	14.43	3.01	1457	92.82
9	6	4	2.415	3.01	90.94	16.47	15.06	3.12	996	58.84
10	5	0	2.421	4.59	72.03	16.23	14.36	3.03	1207	72.32
11	5	2	2.442	4.41	74.31	15.96	14.31	2.99	1471	90.92
12	6	0	2.419	4.88	80.09	17.61	13.62	3.27	989	63.32
13	5	4	2.441	3.15	94.96	15.58	15.57	2.91	1246	78.29

contaminants in landfill waste. Both BGC-MAB and BGC-MAB asphalt concrete underwent testing, with the BGC sample crafted from sieved material and the BGC-MAB asphalt concrete produced using the Marshall mixing method with the optimized asphalt binder and BGC-MAB. The dried samples of control and BGC-MAB asphalt concrete were uniformly crushed and sieved, resulting in approximately 600 g of 9.5 mm sieve-size particles. In the TCLP test, an ethanoic acid solution with a pH of approximately 2.88 was introduced to the sample in a conical flask, maintaining a constant solution-to-sample ratio of 20:1. The sample underwent agitation for 18 h at 24 ± 1 °C using a shaker machine rotating at 30 rotations per minute. This facilitated the reaction of the extraction solution with the sample, potentially leaching out any mobile pollutants. Following thorough mixing, the leachate was filtered into a flask using a 0.60 μ m pore-size syringe filter. Subsequently, the filtered leachate underwent heavy metal testing using Agilent 240FS Atomic Absorption Spectroscopy equipment. The elements studied included As, Ba, Cd, Cr, Cu, Ni, Pb, and Zn, chosen for their significance in previous studies and their environmental impact [33–35]. The TCLP test results were then compared to regulatory limits for heavy metal concentrations in waste materials to ascertain the suitability of BGC-MAB and BGC-MAB asphalt concrete for use in asphalt pavement.

Results and discussion

BGC characterization

X-ray fluorescence

An XRF analysis was utilized to identify the elemental components of BGC, with the oxide components presented in Table 4. Silica oxide emerged as the most abundant component, constituting more than half of BGC's total weight. The heightened concentration of SiO₂ could be attributed to the carbonization process and the utilization of aluminosilicate and metakaolin during BGC production. Minor oxides present in BGC encompass potassium oxide, calcium oxide, iron oxide, aluminum oxide, and phosphorus oxide. These correspond to the diverse metal oxides in the BGC powder blend, affirming that BGC is fundamentally an inorganic material containing the primary elements O, Si, K, Ca, and P. Due to its elevated silica concentration and pozzolanic activity, BGC exhibits pozzolanic behavior. The thermodynamically stable quartz in BGC, when exposed to water, interacts with calcium hydroxide, yielding calcium silicate hydrate gel. This gel holds the potential to enhance the stability and performance of asphalt concrete materials. In summary, BGC's significant silica concentration and reactivity of amorphous silica position it as a viable and sustainable additive within the asphalt pavement industry.

X-ray diffraction

The reaction products of the composite mixture were detected and characterized through XRD analysis. As depicted in Fig. 3, the XRD patterns of the BGC biosorbent exhibited prominent diffraction peaks at 2° and 30°/36°, signifying the stacking of

Table 4 XRF analysis of BGC modifier

Oxides	Al ₂ O ₃	Fe ₂ O ₃	SiO ₂	SO ₃	K ₂ O	CaO	Rb ₂ O	MnO	Cl	MgO	P ₂ O ₅
Content (%)	1.81	1.05	66.07	2.13	17.8	3.71	0.24	0.45	0.97	1.02	4.66

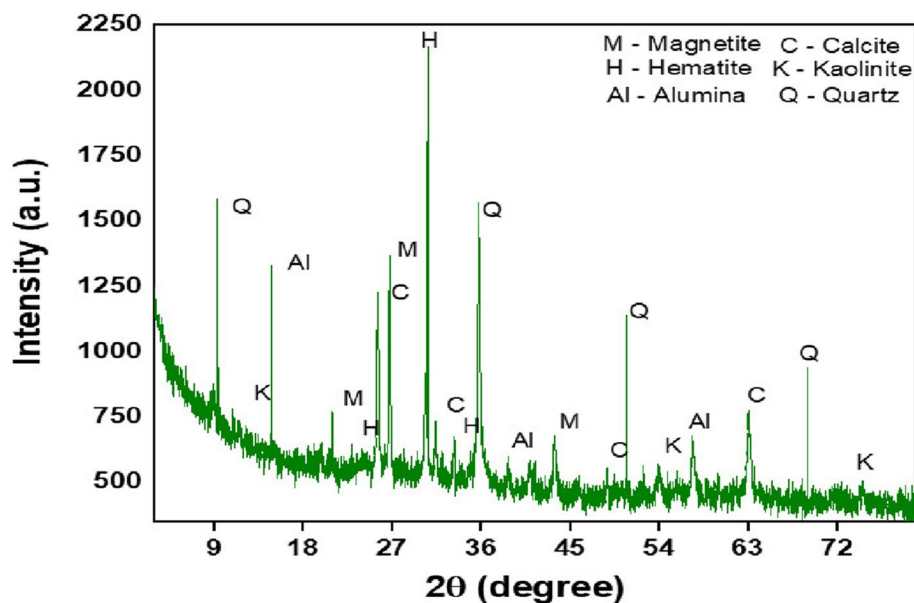


Fig. 3 XRD diffractograms of BGC

inter-graphene layers and the formation of organized graphitic domains, respectively. These patterns unveiled the presence of these elements. Additionally, the peaks associated with the calcite phase (CaCO_3) were linked to the reaction of produced lime with ambient carbon dioxide gas. The significant presence of CH and CSH peaks indicated their evolution as major products. The XRD analysis of the composite mixture confirmed the presence of thermally stable quartz. Metakaolin, a pivotal component of the composite, encompasses quartz, a mineral composed of silicon and oxygen atoms. The inclusion of quartz in the composite contributes to its overall stability and durability. These findings align with the study conducted by Mohamed, et al. [36] which explored and characterized the quartz content in metakaolin-based materials. The insights gained from this analysis enhance our understanding of quartz's role in enhancing composite performance and characteristics, while also affirming the presence of this mineral in the study's BGC modifier.

Scanning electron microscopy

SEM analysis of the BGC sample is presented in Fig. 4. The results reveal a heterogeneous surface characterized by a mixture of various components. The surface displays a naturally rough appearance with thin, uneven layers and finely organized micropetal-like features that are densely interconnected. This observation suggests that the BGC particles possess a larger specific surface area and porosity, as noted by [37]. Additionally, the surface exhibits microporosity, indicating the presence of minute pores or voids. Moreover, the thick structure of the geopolymer matrix contributes to its high mechanical performance. However, the introduction of biochar particles into the geopolymer matrix reduces compactness due to the formation of new interfaces.

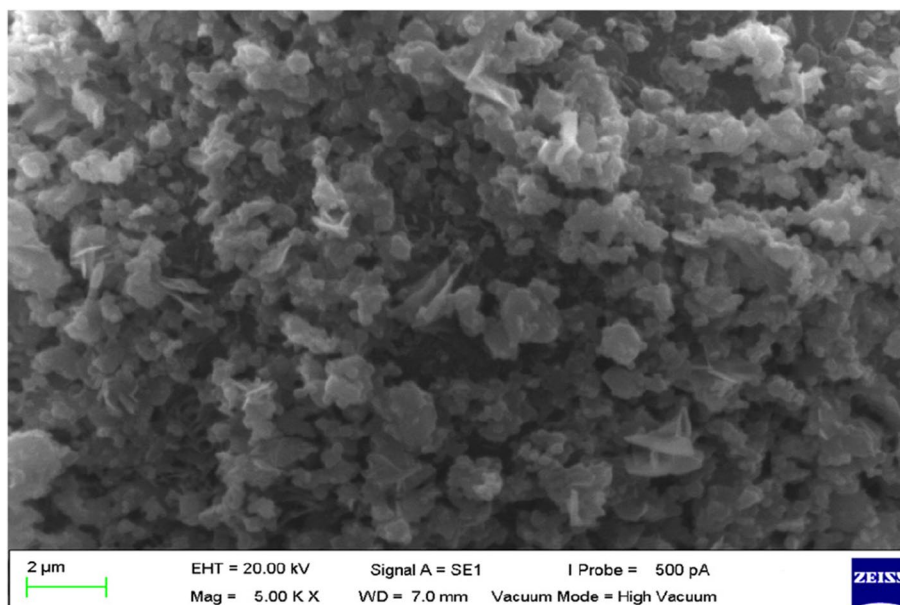


Fig. 4 SEM micrograph of BGC

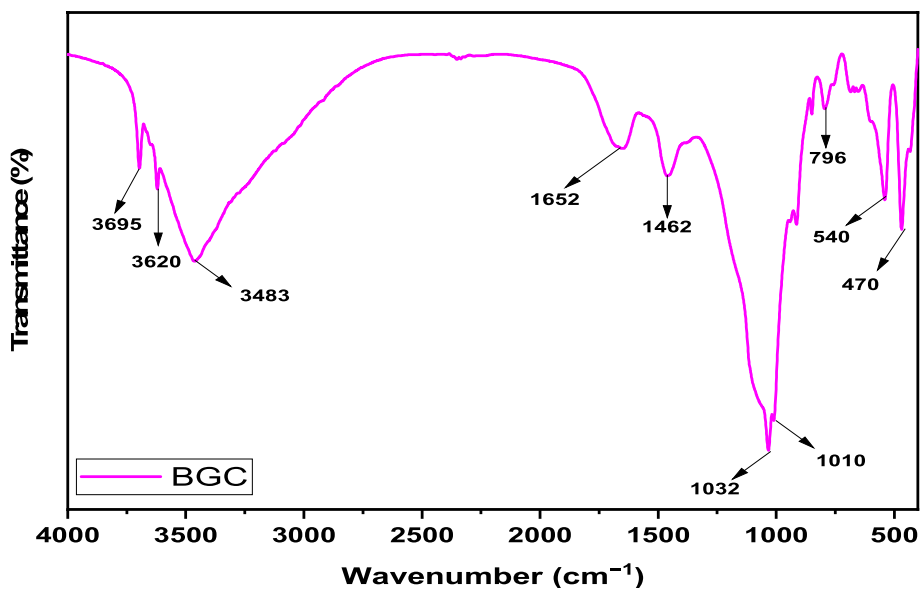


Fig. 5 FTIR spectroscopy of BGC

This suggests that the incorporation of biochar into the BGC matrix significantly alters its compactness, leading to enhanced performance and effectiveness.

Fourier transform infrared spectroscopy

The infrared spectra of BGC (biochar-based geopolymer composite) are illustrated in Fig. 5, revealing several notable peaks. In the range of 470 and 540 cm^{-1} , peaks indicative of Si–O–Si bending vibrations are observed. Notably, the presence of two bands

at 1000 and 1032 cm^{-1} , corresponding to stretching and bending vibrations of (Si–O) in SiO_4 , confirms the occurrence of crystalline phases, including quartz. The Si–O–Al bending vibration is attributed to the presence of alumino-silicate in the BGC material. Additionally, major peaks at 1462, 1652, 3483, 3620, and 3695 cm^{-1} correspond to H–O–H and -OH bond bending and stretching vibrations, suggesting the presence of ambient moisture in the BGC [12]. Furthermore, the extended peak at 1032 cm^{-1} indicates the existence of unique geopolymeric structures, incorporating Si and Al ions [38].

Asphalt binder fundamental properties test

The fundamental properties of both blends were examined to investigate the characteristics of the control (0% BGC) and modified asphalt binder. Table 5 displays these characteristics, which include specific gravity penetration, softening point, ductility, and storage stability.

The introduction of BGC into the unmodified asphalt binder brings about significant changes in its properties. As the BGC content increases from 0 to 4%, there is a noticeable decrease in the penetration grade of the asphalt binder, while the softening point exhibits an inverse relationship by increasing. This shift can be attributed to BGC’s interaction with the asphaltene component and its absorption of the maltene phase, leading to increased rigidity in the asphalt binder. BGC particles, being stiffer than the binder matrix, contribute to reduced blend mobility, resulting in a stiffer asphalt binder. The heightened stiffness, reduced penetration, and increased softening point collectively enhance the resistance to permanent deformation in asphalt concrete produced with such binder mixes, especially under high temperatures. The augmentation of BGC content in the modified asphalt binder improves its penetration index, subsequently enhancing rutting resistance, particularly in high-temperature regions such as Malaysia. Conversely, the increased viscosity and stiffness of the maltene phase diminish the ductility of the asphalt binder mixes. This compromise in ductility serves as a trade-off for the achieved increase in stiffness. Notably, the storage stability of BGC-MAB demonstrates favorable compatibility between bitumen and BGC. The minimal 2.2 °C difference in softening point between the upper and lower portions of the aluminum conduit indicates stability even at elevated temperatures.

Table 5 Fundamental properties of BGC-MAB blends

Fundamental properties	Type of asphalt binder blend				
	0% BGC	1%BGC	2%BGC	3%BGC	4%BGC
Specific gravity	1.022	1.031	1.039	1.046	1.052
Softening point (°C)	49.5	50.3	51.2	51.9	52.7
Ductility (cm)	114	100.7	91.03	80.23	69.95
Penetration (dmm)	87	81	76	73	69
Penetration index	0.106	0.110	0.161	0.224	0.265
Storage stability (°C)	0.21	0.89	1.47	1.95	2.01

RSM statistical analysis for BGC-MAB

The study assessed the parameters of BGC-MAB asphalt concrete, and Table 6 presents the ANOVA analysis, highlighting the reliability of the models. The low coefficient of variation (C.V.) and standard deviation (SD) in the developed models underscore their adequacy. A strong correlation between predicted and laboratory values is indicated by the high coefficient of determination (R^2) for parameters such as BSD, AV, VFA, VMA, Marshall stability, flow, and ITSR, with values of 0.982, 0.982, 0.974, 0.987, 0.983, 0.950, and 0.985, respectively. Additionally, the projected coefficients of determination closely align with the adjusted coefficients of determination, exhibiting a difference of less than 0.2. Assessment using A.P. and the signal-to-noise ratio was conducted to relate the obtained parameters at design samples with the mean estimation discrepancy. Signal-to-noise ratios for BSD, AV, VFA, VMA, Marshall stability, flow, and ITSR all surpassed 4, with values of 26.1620, 28.8539, 24.0467, 32.5029, 29.4124, 28.8937, and 24.8341, respectively. A signal-to-noise ratio exceeding 4 indicates adequate precision, validating the applicability of the models. The developed models, encompassing quadratic and linear elements, efficiently represent the variables without interference. The findings affirm that these models are sufficient and effective for optimizing the properties of BGC-MAB asphalt concrete.

The response equation is expressed by Eqs. 4, 5, 6, 7, 8, 9 and 10, utilizing parameters A and B to denote the asphalt binder and BGC content, respectively. The study investigates the impact of A and B, representing linear relationships in the model. AB signifies cross-linear effects, while A^2 and B^2 represent quadratic effects. The validation of RSM models emphasizes the significance of these terms. The ANOVA hierarchy equations retain A, B, and AB to reflect their influence on the output variables, with positive and negative signs indicating synergistic and antagonistic effects.

$$BSD = 2.44124 - 0.005333A + 0.00883B - 0.01025AB - 0.00834A^2 - 0.00984B^2 \tag{4}$$

$$AV = 4.36448 - 0.34333A - 0.73333B - 0.195AB + 0.25931A^2 - 0.41069B^2 \tag{5}$$

$$VFA = 75.8538 + 5.70667A + 10.6583B - 4.83AB - 2.15828A^2 + 7.18672B^2 \tag{6}$$

$$VMA = 16.0438 + 0.04001A - 0.43833B - 0.075AB + 1.13172A^2 - 0.163276B^2 \tag{7}$$

Table 6 Response fit statistics parameters and verification summary

Responses	Fit statistics parameters						
	SD	Mean	C.V	R^2	Adj. R^2	Pred. R^2	A.P
BSD	0.002	2.43	0.088	0.982	0.969	0.904	26.162
AV	0.110	4.29	2.56	0.982	0.969	0.901	28.854
VFA	2.08	78.17	2.66	0.974	0.955	0.905	24.047
VMA	0.096	16.49	0.583	0.987	0.978	0.911	32.503
Stability	0.102	14.41	0.706	0.983	0.970	0.904	29.411
Flow	0.034	3.00	1.15	0.950	0.940	0.906	28.894
ITSR	1.98	79.36	2.50	0.985	0.974	0.910	24.834
Comment	The models are well-suited for exploring the design space						

$$\text{Marshall stability} = 14.3959 - 0.08833A + 0.643333B + 0.0575AB - 0.60052A^2 + 0.63448B^2 \quad (8)$$

$$\text{Marshall flow} = 2.99692 + 0.18667A - 0.05167B \quad (9)$$

$$\text{ITSR} = 91.0679 - 6.04167A + 2.565B - 4.595AB - 10.6878A^2 - 14.6878B^2 \quad (10)$$

RSM plot assessment of the interactive influence of BGC and asphalt binder content

RSM and CCD collaboratively generated 3D contour surfaces, illustrating the interactions between BGC and asphalt binder content with responses (BSD, AV, VFA, VMA, Marshall stability, flow, and ITSR). The color-coded 3D contour plots use blue to signify low impact, green for moderate impact, and crimson to indicate a significant interaction. Figures 6 and 7 showcase these contour surfaces, providing a visual representation of the relationships between input factors and study responses.

Bulk-specific density

The BSD significantly influences the durability and properties of asphalt concrete, making it a crucial design consideration. The combined impact of the input variables, BGC, and asphalt binder content on BSD is illustrated in Fig. 6(a). According to the 3D surface

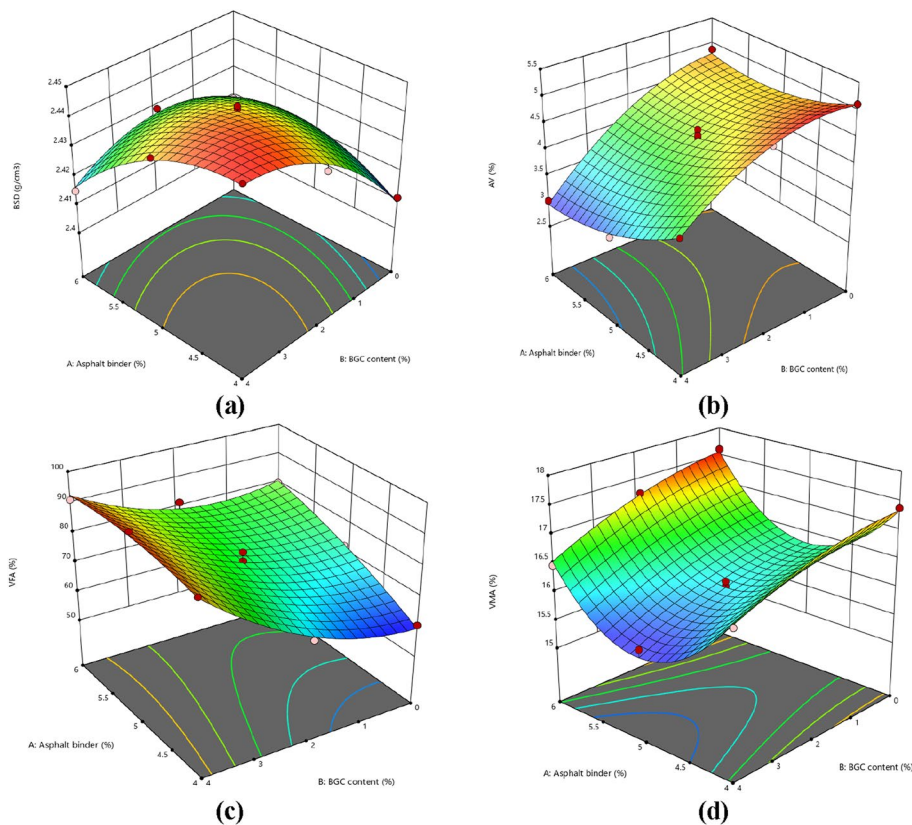


Fig. 6 RSM 3D plot for the synergetic influence of asphalt binder and BGC-MAB content on BSD (a), AV (b), VFA (c), and VMA (d)

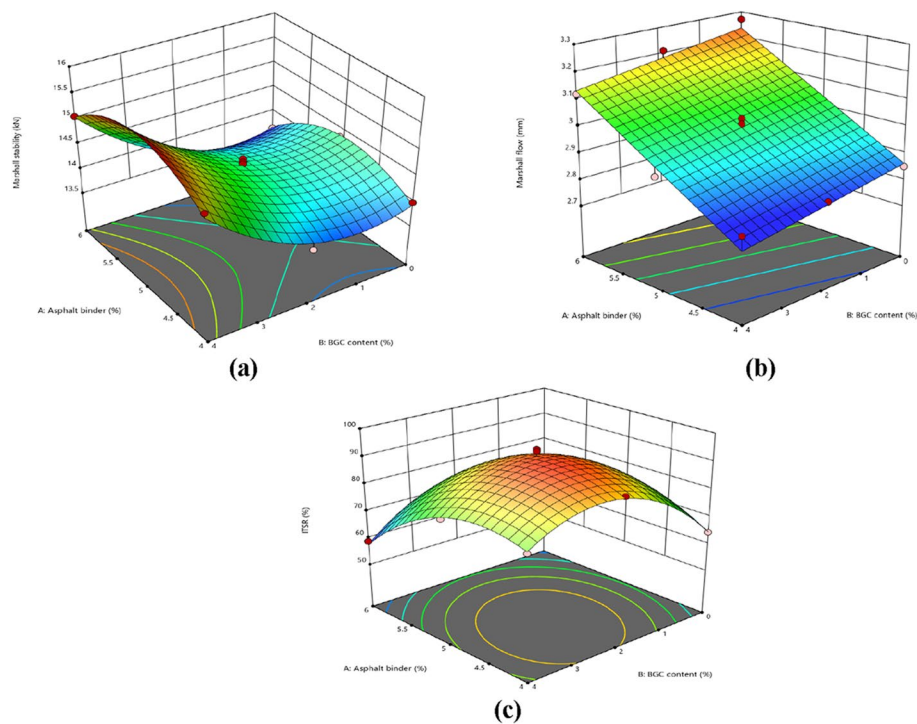


Fig. 7 RSM 2D and 3D plot for the synergetic effect of asphalt binder and BGC-MAB content on Marshall stability (a), Marshall flow (b), and ITSr (c)

plot, both input variables exert a notable influence on BSD, with BSD values increasing as the BGC content rises. Conversely, the impact of asphalt binder content on BSD is minimal, showing only a slight increase until reaching a high value of around 5%. Beyond this threshold, an increase in asphalt binder results in a decline in BSD. The enhanced BSD can be attributed to the augmented viscosity of the modified asphalt binder due to the addition of BGC. The higher viscosity enables better filling of spaces between aggregate particles, leading to improved bonding and increased density, contributing to the heightened BSD of BGC-MAB asphalt concrete. These increased BSD values are also linked to improved workability and viscosity of the asphalt concrete. A similar behavior was observed when palm bio-waste was used as a bitumen modifier [4]. It is noteworthy, however, that the decrease in BSD observed after reaching optimal values is accompanied by a reduction in aggregate cohesiveness. At the point of optimal density, the asphalt binder no longer contributes to aggregate cohesion but instead acts as a medium for aggregate movement.

Air voids

Air voids in asphalt concrete are crucial for determining the optimal asphalt binder content and designing flexible pavement. The synergetic influence of BGC and asphalt binder content on asphalt concrete air voids (AV) is illustrated in the 2D and 3D contour plots in Fig. 6(b). The plots reveal that BGC content exerts a greater influence on AV in BGC-MAB asphalt concrete than asphalt binder content. The 3D graphs depict a significant decrease in AV values with an increase in BGC content in the asphalt binder.

Additionally, as depicted in Fig. 5b, asphalt concrete with 6% asphalt binder and 4% BGC content exhibits the lowest air voids. Reducing air voids is vital for enhancing stiffness and reducing susceptibility to rutting by minimizing the entry of air and water into the asphalt concrete. The dispersion of BGC particles within the asphalt binder significantly affects viscosity and the asphalt concrete's ability to fill gaps. The synergy between BGC particles and asphalt binder results in increased asphalt mixture stiffness, attributed to the enhanced retention and stiffness of BGC, supporting improved asphalt binder coating around the aggregates and enhancing compatibility. Thus, the heightened viscosity and compatibility of BGC-MAB asphalt concrete play a crucial role in achieving the desired performance.

Voids filled with asphalt binder

The VFA parameter plays a crucial role in determining the effective asphalt binder content in asphalt concrete. As the airspaces in asphalt concrete expand, the VFA decreases. The correlation between the input variables and the VFA response for BGC-MAB asphalt concrete is depicted in the 2D and 3D contour plots in Fig. 6(c). These plots highlight a significant relationship between BGC, asphalt binder content, and VFA values. Both BGC content and asphalt binder content impact VFA in asphalt concrete, with BGC content exhibiting a greater influence. The increase in VFA is attributed to filling the spaces between coarse aggregate particles with fine BGC particles, enhancing asphalt concrete compaction and densification. Moreover, elevating the asphalt binder percentage improves VFA by facilitating better filling of voids within the mixture [23]. These modifications result in fewer air spaces and enhanced asphalt concrete performance. It is noteworthy that the VFA content in BGC-MAB asphalt concrete noticeably increases when the asphalt binder percentage is between 5.5 and 6%, and the BGC content is between 3 and 4%. This increase suggests that these specific BGC-MAB asphalt concrete mixtures will have fewer air voids, thereby contributing to the durability and moisture resistance of asphalt pavement.

Voids in mineral aggregate

The VMA parameter plays a crucial role in determining whether the asphalt binder layer coating is sufficient to protect the asphalt pavement from water damage and tire abrasion. The 3D contour plots in Fig. 6(d) illustrate the simultaneous effects of BGC content and asphalt binder content on VMA. It was observed that increasing the asphalt binder percentage from 4 to 5% resulted in a significant decrease in VMA, while further increasing it from 5 to 6% led to a notable increase in VMA. In contrast, increasing the BGC content from 0 to 4% resulted in a slight decrease in VMA. This trend suggests that the asphalt binder content has a greater influence on VMA than the BGC content, as VMA readings show only minor fluctuations with increasing BGC content. Interestingly, the asphalt concrete with the highest BGC content exhibited the smallest decrease in VMA. These observations are attributed to the accumulation of BGC particles within the asphalt concrete, particularly as the excess BGC content in the asphalt binder increases. These clusters absorb the light component of the asphalt binder, limiting aggregate absorption of the asphalt binder and resulting in lower VMA values. It is noteworthy that the VMA levels were consistently higher than the JKR standard's minimum

limit of 14% across all BGC content [39]. Adequate VMA not only increases the stability of the asphalt concrete but also ensures proper aggregate coating. This implies that the mixture can withstand high-stress changes, preventing the displacement of the asphalt binder and reducing air voids due to greater compaction during its service life.

Marshall stability

When developing and producing an asphalt pavement-wearing course, Marshall stability is critical. The ability of an asphalt mixture to withstand deformation and stresses caused by traffic loading is directly related to its strength. Therefore, asphalt concrete must be sufficiently stable to withstand dynamic vehicular stresses [40]. The 3D RSM plots of the Marshall stability model are shown in Fig. 7(a), illustrating the combined effect of BGC and asphalt binder content. The contour lines in the model are semi-elliptical, indicating a strong relationship between BGC content and asphalt binder content. However, BGC content has had a significantly greater impact than asphalt binder content. Furthermore, the graphs show that stability improved as the asphalt binder percentage increased from 4 to 5.5%, and the BGC content increased from 0 to 3%. However, when the asphalt binder content exceeds 5.4%, stability decreases. This demonstrates that an excessive amount of asphalt binder degrades mixture stability, emphasizing the importance of achieving an optimal amount of asphalt binder in asphalt concrete. According to the plot, the optimal range for asphalt binder content is between 5 and 5.5%. Excessive asphalt binder content may reduce aggregate interconnectivity and overall stability. However, increasing the BGC content from 3 to 4% significantly improves stability. This improved stability can be attributed to BGC's ability to enhance aggregate bonding, thereby increasing asphalt concrete strength, and enabling it to withstand higher vehicular stresses. Similar behavior was observed when palm bio-waste was used as a mixture modifier [4]. This suggests that the presence of BGC-MAB improves asphalt mixture performance by occupying and strengthening weaker areas within asphalt mixture.

Marshall flow

Marshall flow is the ability of asphalt concrete to deform without breaking when progressive loading is applied at a specific rate [41]. Asphalt concrete with larger flow is more susceptible to pressure deformation, whereas those with small flow are rigid and prone to cracking [40]. In the Marshall flow model, Fig. 7(b) depicts the 3D linear synergistic relationship between BGC content and asphalt binder content. The RSM created a 3D surface map that demonstrates that both BGC content and asphalt binder content have a comparable influence. The flow increased from 4 to 6% asphalt binder content and decreased slightly as BGC content increased. Because of their linear relationship, increasing the BGC and asphalt binder content results in higher flow values in BGC-MAB asphalt blends. Unmodified asphalt concrete flow generally increases with increasing asphalt binder content, implying that the addition of asphalt binder reduces intra-aggregate friction, causing them to loosen under vehicular pressure. However, the presence of viscous asphalt binder, due to the inclusion of BGC, improves the stiffness and internal friction among mineral aggregates in the asphalt mixture, resulting in lower flow values.

Water susceptibility test

The indirect tensile strength ratio (ITSR) of asphalt concrete reflects its water sensitivity, as water infiltration can disrupt the bonding between asphalt and mineral aggregates, leading to a loss of strength over time [42]. The 3D synergistic influence of BGC content and asphalt binder content on ITSR is depicted in Fig. 7(c). According to the 3D surface plot, both BGC content and asphalt binder have a significant effect on the water damage resistance of asphalt concrete, with BGC content having a stronger effect. The addition of biochar-based geopolymer to BGC increases the asphalt binder, resulting in increased viscosity and a stiffer asphalt binder. This enhances the durability and strength of the asphalt concrete in the presence of water infiltration, similar to the behavior observed when palm bio-waste was used as a bitumen modifier [4]. Raising the BGC content from 0 to 3.5% and the asphalt binder content from 4 to 5% resulted in a significant improvement in the water resistance of the asphalt mixture. However, as the asphalt binder content increased from 5 to 6% and the BGC content increased from 3.5 to 4%, the water damage resistance decreased marginally. The optimal range for water damage resistance, as illustrated by the bright reddish sections in the 3D contour, is between 4.6 and 5.5% asphalt binder and 2.5 and 3.5% BGC content, according to the 3D RSM plot.

BGC-MAB asphalt concrete numerical multi-criteria optimization

To identify optimal input factors for various responses, we employed RSM software and multi-criteria optimization, concentrating on enhancing stability and water resistance for longer-lasting asphalt pavement based on PWD standard criteria. Desirability, rated on a scale of 0 to 1, assessed how well-predicted responses aligned with model boundaries. The input variables and response ramps utilized during optimization are depicted in Fig. 8. With a desirability of 0.936, the software generated the best possible blend. The results indicate that a BGC content of 2.72% and asphalt binder content of 4.56% meet the design parameters for increasing the stability and water resistance of BGC-MAB asphalt concrete. Additional experiments with triplicate samples were conducted to validate the correctness and dependability of the

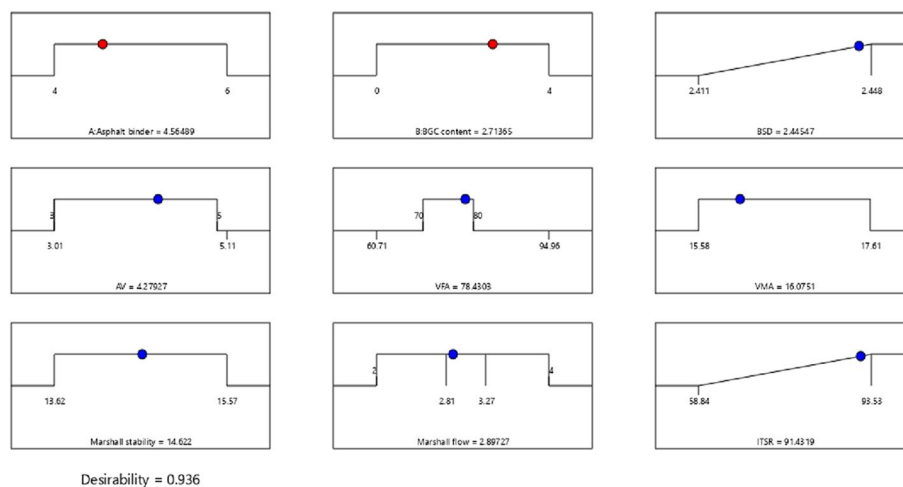


Fig. 8 Numerical multi-objective optimization ramps for BGC-MAB asphalt concrete

RSM-developed model. Using the optimal input factors determined by multi-criteria optimization evaluation, the predicted responses were compared to the experimental values. To assess prediction accuracy, the prediction percentage error between the actual and predicted values was calculated [43]. This evaluation provided useful information about the model's predictability while also demonstrating its adequacy and consistency with experimental data [44]. The optimized model verification for experimental and predicted responses, as well as the percentage error difference, is shown in Table 7. Furthermore, when comparing experimental and model-predicted values, the absolute error was 3.88%, which was well within the allowed range of less than 5%. These results validate the model's high accuracy in forecasting BGC-MAC asphalt concrete responses, indicating its dependability and precision.

Microstructural analysis

Fourier transform infrared spectroscopy

The FTIR spectra of the control asphalt binder, optimized BGC-MAB, and BGC are shown in Fig. 9. Notably, the peaks in the control binder coincided with those in the BGC-MAB, showing that the two molecules have similar molecular structures. Several peaks related to different functional groups in the asphalt binder. The peaks at 2849 cm^{-1} and 2924 cm^{-1} were assigned to CH_3 stretching (aliphatic branched), whereas the peaks at 1458 cm^{-1} were attributed to CH_2 bending of $-(\text{CH}_2)_n-$ aliphatic index. The existence of a peak ranging from 1560 to 1630 cm^{-1} suggested the presence of aromatic compounds, notably benzene ring ($\text{C}=\text{C}$) structures, within the binder. Furthermore, a small signal at 2849 to 2924 cm^{-1} were found, representing the CH_3 stretching (aliphatic branched). The degree to which the modifier (BGC) interacts with the asphalt binder determines the quality and performance of the modified asphalt. This interaction is critical in determining the modified asphalt binder's properties. The major components of BGC-MAB were aromatic and hydrocarbon chemicals. The presence of $\text{Si}(\text{OH})_4$ was suggested by an absorption stretch around 1032 cm^{-1} indicating the interaction of BGC's silica with the binder. These findings are consistent with previous studies [45, 46]. The measured absorption frequency peaks and shifts illustrate BGC's influence on asphalt binder properties, resulting in a different chemical environment in BGC-MAB compared to the control binder, influencing its performance.

Table 7 Optimized model verification for experimental and predicted responses

Input factors	Response	Model predicted	Experimental	Error (%)
Asphalt binder = 4.56	BSD (g/cm ³)	2.445	2.542	3.97
	AV (%)	4.28	4.13	3.51
	VFA (%)	78.43	75.21	4.11
	VMA (%)	16.07	15.43	3.98
	Marshall stability (kN)	14.62	14.09	3.63
BGC content = 2.72	Marshall flow (mm)	2.897	3.02	4.25
	ITSR (%)	91.43	94.79	3.68
	Average error (%)	3.88		

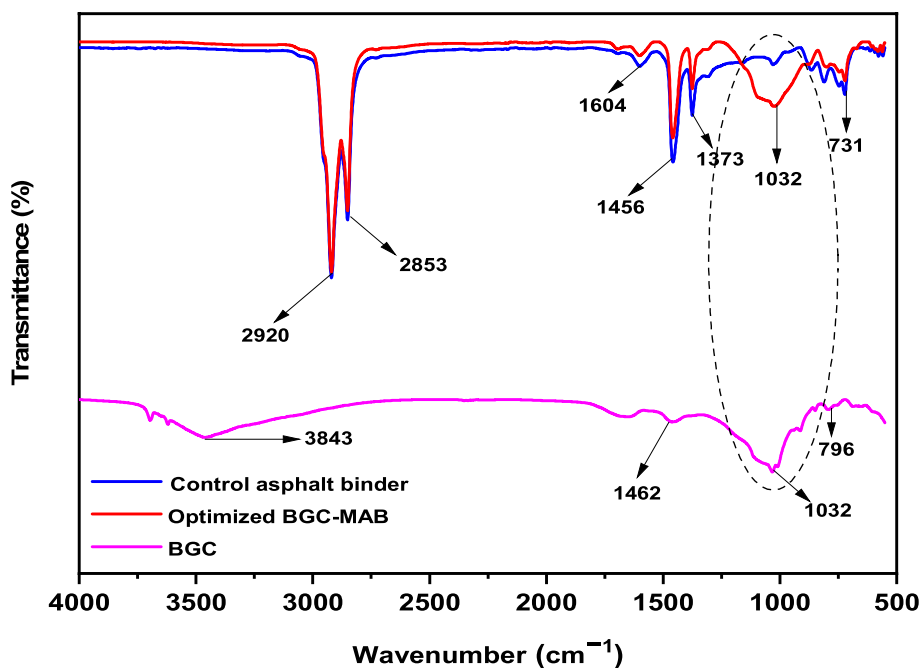


Fig. 9 Combine BGC, control asphalt binder, and BGC-MAB FTIR spectra

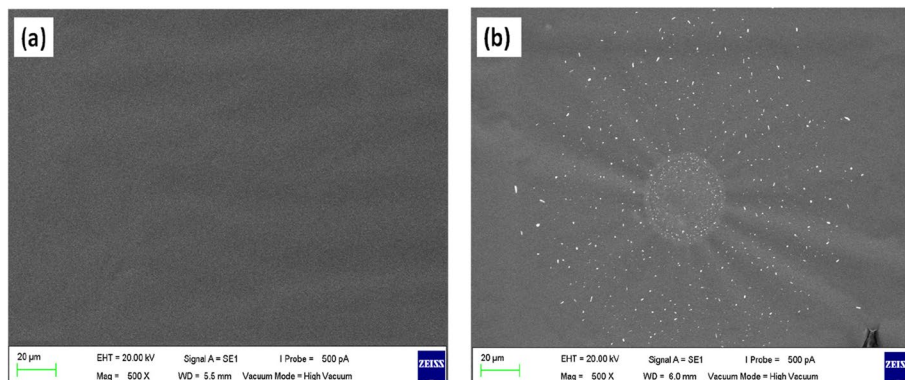


Fig. 10 SEM micrograph of (a) control asphalt binder and (b) optimized BGC-MAB

Scanning electron microscopy

Figure 10 displays SEM images used in the investigation to analyze the control asphalt binder and optimized BGC-MAB at a magnification of 20 times. BGC exhibits a rough surface appearance and a well-developed pore structure. The smooth surface of the control asphalt binder is evident in Fig. 10; however, the SEM image of optimized BGC-MAB illustrates the dispersion and intricate network structure of BGC within the asphalt binder. The visual micrograph describes the stiffening area as the section of the asphalt binder’s resin area containing BGC particles. The appearance of white particles in the graphs indicates stiffening zones in the BGC-MAB. Ma et al. [47] found a similar result when using biochar to modify and improve the rheological properties of asphalt binder. Additionally, as the BGC chemically reacted with

the asphalt binder, it resulted in the formation of a novel network structure; the BGCF-MAB also functions as a single entity, as shown in the SEM micrographs. Furthermore, the presence of a porous structure increases the specific interface area, improving the interaction between the asphalt binder constituent and the BGC and thus compatibility with the asphalt binder. BGC particles' rough surface fills gaps and quickly interlocks with the asphalt binder, forming a framework structure that improves the fundamental properties of the asphalt binder. These data support the BGC-MAB blend's lower penetration value, improved softening point, ductility, and penetration index.

Influence of immersion period on the durability of control and BGC-MAB asphalt concrete

The ITSr was utilized to evaluate the water permeability of asphalt concrete. In Fig. 11, the impact of BGC on ITSr is illustrated for both control and BGC-MAB asphalt concrete after 1 to 6 days of water submersion. In dry conditions, ITSr increased from 80.3 (control) to 91.43% (BGC-MAB). However, as the immersion time increased in both cases, ITSr decreased. Water penetration into the samples resulted in issues at the asphalt binder-aggregate interface. After the first day of immersion, the control ITSr fell below the permitted threshold (>80%), but BGC-MAB asphalt concrete maintained acceptable ITSr levels throughout. According to the findings, the addition of BGC-MAB to asphalt concrete significantly reduced water-related weakening by increasing ITSr and enhancing the asphalt concrete's resistance to moisture damage. The increased durability is attributed to the water reaction aided by the presence of BGC-MAB in the asphalt concrete. After 6 days of immersion, the control asphalt concrete experienced a

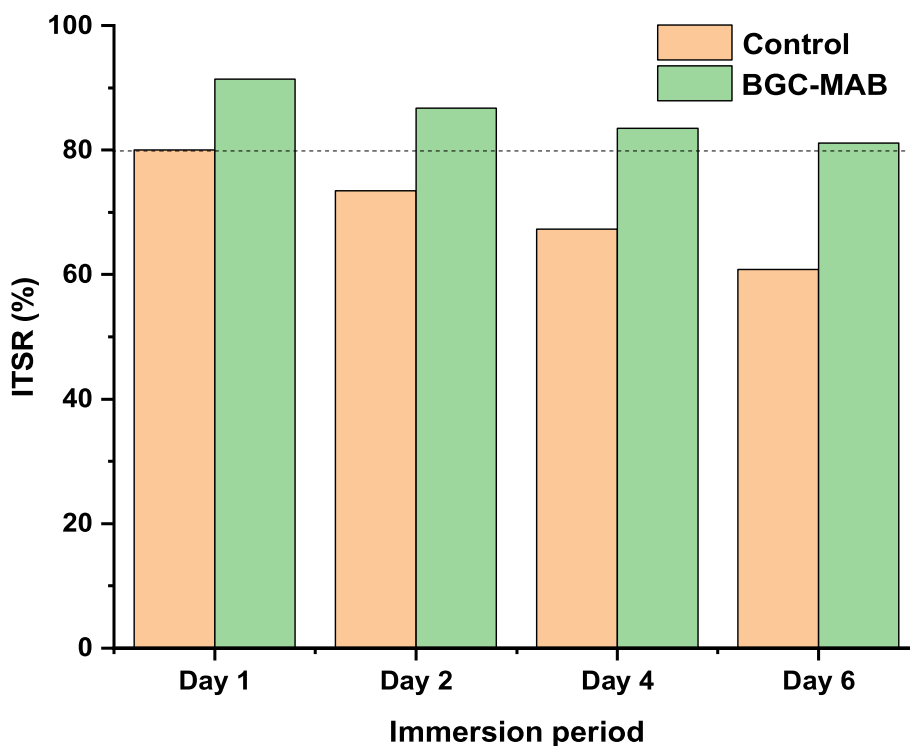


Fig. 11 Effect of water immersion period on the ITSr of control and BGC-MAB asphalt concrete

20% decrease in ITSR values, while the BGC-MAB asphalt concrete had a 12% decrease in ITSR values. A similar pattern was observed by Yaro et al. [4] in a study where palm waste powder was used to improve asphalt mixtures water resistance.

TCLP results for BGC, control, and BGC-MAB asphalt concrete

The concentrations of heavy metals in both BGC and BGC-MAB asphalt concrete were assessed and compared to EPA allowable limits. Table 8 displays the results, indicating that all heavy metal concentrations were below the permissible limits. Arsenic concentrations were highest in BGC, possibly due to the presence of potassium oxide (K₂O) from palm waste and rice straw incineration, leading to the formation of amorphous minerals. Copper (Cu), nickel (Ni), and zinc (Zn) levels were lower than expected, likely due to vaporization during the combustion process. Cadmium (Cd), chromium (Cr), and lead (Pb) concentrations were extremely low, suggesting vaporization or redistribution in a stable crystalline form. The heavy metal levels in both control and BGC-MAB asphalt concretes were well below TCLP regulatory standards. While asphalt concrete is effective at retaining components like Cd, Pb, Cu, and Zn [48], Pb’s impact on subgrade moisture and properties is a concern. Nevertheless, Pb leaching values were found to be modest in this study. Moreover, Zn, a soluble metal found in the atmosphere, water, and soil, exhibited higher leaching values in this study, attributed to the presence of asphalt binder and ethanoic acid extraction liquid. Additionally, nickel (Ni) content was higher only in the control asphalt concrete, with lower leaching values in BGC-MAB asphalt concrete. Ni is known for its environmental resistance, potentially affecting subgrade characteristics and water content [49]. Finally, chromium (Cr) is a highly toxic metal, but its levels in BGC-MAB asphalt concrete were significantly below regulatory limits. Comparing BGC to BGC-MAB asphalt concrete, the latter showed a significant reduction in heavy metal leaching, indicating effective hazardous metal stabilization by the asphalt mixture. Therefore, it can be concluded that BGC can be safely used in the pavement industry without posing significant environmental risks during the pavement’s service life, similar to findings observed with sludge filler in asphalt concrete [48].

Conclusions

This study employs a statistical approach, RSM, to examine the impact of different asphalt binder and BGC content on the volumetric properties, Marshall parameters, and water damage resistance of asphalt concrete. The conclusions drawn from the analysis of both experimental data and RSM results are as follows:

Table 8 BGC and BGC-MAB asphalt concrete leaching results

Variable	Leaching value (mg/L)							
	As	Ba	Cd	Cr	Cu	Ni	Pb	Zn
USEPA limits	5	100	0.11	0.60	-	11	0.75	4.3
BGC	3.45	0.29	-	0.002	1.09	0.19	0.001	0.51
Control sample	3.71	0.52	0.087	0.009	0.021	0.204	0.029	0.031
BGC-MAB sample	3.78	0.45	0.091	0.021	0.019	0.185	0.031	0.024

- The incorporation of BGC into the asphalt binder led to an increase in PI values, enhancing stiffness and resilience to low-temperature challenges. However, a higher BGC content resulted in reduced asphalt binder ductility, attributed to heightened viscosity and stiffness in the maltene phase.
- The RSM models employed to analyze the volumetrics, Marshall parameters, and water damage resistance of asphalt concrete yielded highly significant results. These outcomes affirm the reliability and effectiveness of the models in accurately capturing the relationships between variables and responses. Notably, the R^2 values surpassed 0.90, precision values exceeded 4, and p -values remained low.
- Numerical optimization through RSM resulted in a notable desirability value of 0.936, suggesting an optimal blend with 4.56% asphalt binder and 2.71% BGC content. Subsequent validation testing confirmed these optimized parameters with an error margin of less than 5%, affirming the model's accuracy and the significance of the optimized parameters in enhancing the qualities of asphalt concrete.
- The incorporation of BGC-MAB contributed to increased stiffness, enhancing resistance to deformation and overall stability. This improvement can be attributed to the hydration process of BGC, which enhances the mix's stiffness and, consequently, its ability to withstand degradation induced by water.
- The FTIR study of BGC-MAB highlights Si–O–Si stretching induced by BGC in the asphalt binder. SEM analysis further confirms the dispersion of BGC and the micro-network structure within the binder. The micrograph identifies the stiffening zone in the resin region, containing BGC particles.
- Leaching tests utilizing TCLP revealed that both BGC and BGC-MAC asphalt concrete met USEPA standards. This study demonstrates that leaching has no environmental impact, enabling BGC's usage as a sustainable modifier in the pavement sector and aligning with environmental responsibility concepts and sustainability goals.

Abbreviations

RSM	Response surface methodology
PWD	Public work department
BGC	Biochar-based geopolymer composite
CCD	Central composite design
POFA	Palm oil fuel ash
PMG	POFA metakaolin geopolymer
RSB	Rice straw-based biochar
BGC-MAB	BGC-modified asphalt binder
OAC	Optimal asphalt binder content
AC14	Asphalt concrete with a nominal maximum aggregate size of 14 mm
ITS	Indirect tensile strength
ITSR	ITS ratio
ANOVA	An analysis of variance
CV	Coefficient of variance
SD	Standard deviation
A.P	Adequate precision
BSD	Bulk specific density
AV	Air voids
VFA	Voids filled with asphalt binder
VMA	Voids filled with mineral aggregates
2D	Two-dimensional
3D	Three-dimensional

Acknowledgements

The authors wish to express their heartfelt appreciation to the Universiti Teknologi PETRONAS Centre for Graduate Studies and Ahmadu Bello University Zaria for their invaluable support through the graduate assistance initiative.

Authors' contributions

All authors contributed significantly to the study in the areas of conceptualization, methodology, analysis, optimization, validation, and manuscript writing. NSAY: conceptualization, data curation, formal analysis, investigation, methodology, software, writing of the original draft. MHS: project administration, resources, supervision. NZH: project administration, resources, supervision. AU: software, validation, visualization. LET: writing—review and editing. IA: writing—review and editing. AHJ: writing—review and editing. All the authors jointly conducted a formal analysis of the laboratory outcome. The final manuscript was read and approved by all authors.

Funding

No funding was received for conducting this study.

Availability of data and materials

Data can be shared upon request as a basic requirement dictated by Springer rules.

Declarations

Competing interests

The authors declare no competing interests.

Received: 12 October 2023 Accepted: 19 November 2023

Published online: 13 December 2023

References

1. Wang HP, Guo YX, Wu MY, Xiang K, Sun SR (2021) Review on structural damage rehabilitation and performance assessment of asphalt pavements. *Rev Adv Mater Sci* 60(1):438–449
2. Jameel MS, Ahmad N, Badin G, Khan AH, Ali B, Raza A (2023) Comparison of hydrated lime, paraffin wax and low-density polyethylene modified bituminous binders: a perspective of adhesion and moisture damage. *Int J Pavement Eng* 24(1):2168659
3. Guo T et al (2021) Road performance and emission reduction effect of graphene/tourmaline-composite-modified asphalt. *Sustainability* 13(16):8932
4. Yaro NSA, et al (2022) Feasibility evaluation of waste palm oil clinker powder as a fillers substitute for eco-friendly hot mix asphalt pavement. *Int J Pavement Res Technol* 1–14. <https://link.springer.com/article/10.1007/s42947-022-00247-x>, https://scholar.google.com/scholar?cites=17013905005568408829&as_sdt=2005&sciodt=0.5&hl=en
5. Jameel MS, Abubakar HM, Raza A, Iqbal S, Khalid RA (2022) Effect of aging on adhesion and moisture damage of asphalt: a perspective of rolling bottle and bitumen bond strength test. *Int J Pavement Res Technol* 15(1):233–242
6. Sodeyfi S, Kordani AA, Zarei M (2022) Moisture damage resistance of hot mix asphalt made with recycled rubber materials and determining the optimal percentage with an economic approach. *Int J Pavement Res Technol* 15(4):970–86
7. Chen Q, Lu Y, Wang C, Han B, Fu H (2022) Effect of raw material composition on the working performance of waterborne epoxy resin for road. *Int J Pavement Eng* 23(7):2380–2391
8. Badin G, Ahmad N, Ali HM, Ahmad T, Jameel MS (2021) Effect of addition of pigments on thermal characteristics and the resulting performance enhancement of asphalt. *Constr Build Mater* 302:124212
9. Yaro NSA et al (2023) A comprehensive review of biochar utilization for low-carbon flexible asphalt pavements. *Sustainability* 15(8):6729
10. Ma C et al (2023) Property evaluation of magnesia-based cement emulsified asphalt mortar (MCAM) as pavement repair material. *Int J Pavement Eng* 24(1):2209264
11. Yaro NSA, Sutanto MH, Habib NZ, Napiah M, Usman A, Muhammad A (2022) Comparison of response surface methodology and artificial neural network approach in predicting the performance and properties of palm oil clinker fine modified asphalt mixtures. *Constr Build Mater* 324:126618
12. Al-Mahbashi NMY et al (2022) Bench-scale fixed-bed column study for the removal of dye-contaminated effluent using sewage-sludge-based biochar. *Sustainability* 14(11):6484
13. Zhou X, Adhikari S (2019) Flow-induced crystallization of biochar in bio-asphalt under various aging conditions. *Sci Total Environ* 695:133943
14. Çeloğlu ME, Mehmet Y, Kök BV, Yalcin E (2016) Effects of various biochars on the high temperature performance of bituminous binder. *Proceedings of the 6th Eurphalt & Eurobitume Congress*
15. Ghasemi H, Yazdani H, Rajib A, Fini EH (2022) Toward carbon-negative and emission-curbings roads to drive environmental health. *ACS Sustain Chem Eng* 10(5):1857–1862
16. Milad A et al (2021) Utilisation of waste-based geopolymer in asphalt pavement modification and construction—a review. *Sustainability* 13(6):3330
17. Shehata N, Mohamed O, Sayed ET, Abdelkareem MA, Olabi A (2022) Geopolymer concrete as green building materials: recent applications, sustainable development and circular economy potentials. *Sci Total Environ* 836:155577
18. Ismail MA (2011) Creep properties of geopolymer bituminous mixtures
19. Ahyudanari E, Ekaputri JJ, Tardas M (2016) Analysis of coal waste solidification as an alternative filler material in asphalt concrete mixture. *Mater Sci Forum* 841:65–71 *Trans Tech Publ*
20. Aditama AT, Ekaputri JJ, Ahyudanari E (2019) Analysis of aggregate gradation to improve the characteristics of geopolymer based asphalt concrete. *IPTeK J Technol Sci* 29(3):86–90

21. Yaro NSA, Napiah MB, Sutanto MH, Usman A, Murana AA, Rafiq W (2021) Effect of palm oil clinker powder-based geopolymer on bitumen and asphalt mixture properties. 2021 Third International Sustainability and Resilience Conference: Climate Change. IEEE, New York, pp 310–315
22. Jameel MS, Khan AH, urRehman Z, Tarar MA (2023) Evaluation of performance characteristics of asphalt mixtures modified with renewable oils and reclaimed asphalt pavement (RAP). *Constr Build Mater* 375:130925
23. Yaro N et al (2022) Geopolymer utilization in the pavement industry-an overview. *IOP Conf Ser Earth Environ Sci* 1022(1):012025 IOP Publishing
24. Yaro N, Napiah M, Sutanto M, Usman A, Saeed S, Kaura J (2021) Influence of modification mixing parameters on conventional properties of palm oil clinker fine (POCF)-modified bitumen. *Mater Today* 48(4):771–777
25. Raya JK (2008) Standard specification for road works. JKR/SPJ/rev2005
26. Jagaba AH et al (2023) Biochar-based geopolymer nanocomposite for COD and phenol removal from agro-industrial biorefinery wastewater: kinetic modelling, microbial community, and optimization by response surface methodology. *Chemosphere* 339:139620
27. Astm A (2015) D6927–15 standard test method for marshall stability and flow of asphalt mixtures. ASTM International, West Conshohocken
28. Mohammed BS, Haruna S, Liew M (2019) Optimization and characterization of cast in-situ alkali-activated pastes by response surface methodology. *Constr Build Mater* 225:776–787
29. Bala N, Kamaruddin I, Napiah M, Sutanto MH (2019) Polymer nanocomposite-modified asphalt: characterisation and optimisation using response surface methodology. *Arab J Sci Eng* 44(5):4233–4243
30. Yaro NSA, Napiah MB, Sutanto MH, Usman A, Saeed SM (2021) Modeling and optimization of mixing parameters using response surface methodology and characterization of palm oil clinker fine modified bitumen. *Constr Build Mater* 298:123849
31. Usman A, Sutanto MH, Napiah M, Zoorob SE, Yaro NSA, Khan MI (2021) Comparison of performance properties and prediction of regular and gamma-irradiated granular waste polyethylene terephthalate modified asphalt mixtures. *Polymers* 13(16):2610
32. Jagaba AH et al (2023) Trend and current practices of coagulation-based hybrid systems for pulp and paper mill effluent treatment: mechanisms, optimization techniques and performance evaluation. *J Clean Product* 429:139543
33. Azadgoleh MA et al (2022) Characterization of contaminant leaching from asphalt pavements: a critical review of measurement methods, reclaimed asphalt pavement, porous asphalt, and waste-modified asphalt mixtures. *Water Res* 219:118584
34. Zhao Y, Zhu Y-T (2019) Metals leaching in permeable asphalt pavement with municipal solid waste ash aggregate. *Water* 11(10):2186
35. Rahmad S et al (2022) Assessment of metal leaching from rediset-polymer modified asphalt binder on groundwater and soil contamination. *Case Stud Constr Mater* 16:e01108
36. Mohamed O, El-Gamal S, Farghali A (2022) Utilization of alum sludge waste for production of eco-friendly blended cement. *J Mater Cycles Waste Manage* 24(3):949–970
37. Chen H, Zhang YJ, He PY, Li CJ, Liu LC (2020) Novel activated carbon route to low-cost geopolymer based porous composite with high mechanical resistance and enhanced CO₂ capacity. *Microporous Mesoporous Mater* 305:110282
38. Sarkar C, Basu JK, Samanta AN (2019) Experimental and kinetic study of fluoride adsorption by Ni and Zn modified LD slag based geopolymer. *Chem Eng Res Des* 142:165–175
39. Raya JK (2008) JKR/SPJ/S4; Standard specification for road works. Public Works Department, Kuala Lumpur, Malaysia. https://scholar.google.com/scholar_lookup?title=Standard%20Specification%20for%20Road%20Works&publication_year=2008&author=Jkr%2C%20spj%2C%20-s4%2C
40. Usman A, Sutanto M, Napiah M, Zoorob S, Khan M, Ibrahim M (2020) Application of gamma irradiation on polyethylene terephthalate (PET) for use in asphaltic concrete mixtures as aggregates replacement. *IOP Conf Ser Earth Environ Sci* 498(1):012008 IOP Publishing
41. Yaro N et al (2021) Evaluation of the impact of short-term aging on volumetric and Marshall properties of palm oil clinker fine modified asphalt concrete (POCF-MAC). *J Phys Conf Ser* 1793(1):012054 IOP Publishing
42. Hainin M et al (2018) Performance of hot mix asphalt mixture incorporating kenaf fibre. *IOP Conf Ser Earth Environ Sci* 140(1):012092 IOP Publishing
43. Saeed SM et al (2021) Optimization of rubber seed oil content as bio-oil rejuvenator and total water content for cold recycled asphalt mixtures using response surface methodology. *Case Stud Constr Mater* 15:e00561
44. Al-dhawi BNS et al (2023) Adsorptive removal of boron by DIAION™ CRB05: characterization, kinetics, isotherm, and optimization by response surface methodology. *Processes* 11(2):453
45. Hussein AA, Jaya RP, Hassan NA, Yaacob H, Huseien GF, Ibrahim MHW (2017) Performance of nanoceramic powder on the chemical and physical properties of bitumen. *Constr Build Mater* 156:496–505
46. Sembiring S, Riyanto A, Situmeang R, Sembiring Z (2019) Bituminous composite comprising amorphous silica from rice husks. *Ceramics Silikat* 63(3):277
47. Ma F et al (2022) Biochar for asphalt modification: a case of high-temperature properties improvement. *Sci Total Environ* 804:150194
48. Hasan M, Al Biruni MT, Afia A, Ahmed T (2022) Utilization of sludge from water treatment plant as a filler material in pavements. *J Mat Cycles Waste Manag* 24(6):2656–2668
49. Kayhanian M, Vichare A, Green PG, Harvey J (2009) Leachability of dissolved chromium in asphalt and concrete surfacing materials. *J Environ Manage* 90(11):3574–3580

Publisher's Note

Springer Nature remains neutral with regard to jurisdictional claims in published maps and institutional affiliations.